Articles

Studies of Sequence-Specific DNA Binding, DNA Cleavage, and Topoisomerase I Inhibition by the Dimeric Chromomycin A_3 Complexed with Fe^{II}†

Ming-Hon Hou,*,‡,§,|| Wen-Je Lu,‡ Hsin-Ying Lin,|| and Jeu-Ming P. Yuann⊥

Biotechnology Center, National Chung Hsing University, Taichung, 402 Taiwan, Institute of Bioinformatics, National Chung Hsing University, Taichung, 402 Taiwan, Department of Life Science, National Chung Hsing University, Taichung, 402 Taiwan, and Department of Biotechnology, Ming Chuan University, Taoyuan County, 333 Taiwan

Received September 20, 2007; Revised Manuscript Received January 22, 2008

ABSTRACT: Chromomycin A_3 (Chro) has been evidenced to exhibit much higher binding affinity toward Fe^{II} by forming a highly stable 2:1 drug/metal complex, compared to its structural analogue, mithramycin (Mith). Different properties of the [$(Chro)_2-Fe^{II}$] complex acting on DNA, such as sequence specificity, DNA cleavage, and topoisomerase I (TopI) inhibition were studied. Kinetic analyses of surface plasmon resonance showed that the affinity of the [$(Chro)_2-Fe^{II}$] complex upon binding to hairpin DNA duplexes containing various tetranucleotide sequences follows the order: GGCC > CGCG > CCGG ~ GCGC > AGCT > ACGT > TGCA > TCGA. According to circular dichroism (CD) studies, most hairpin DNA duplexes appeared to retain their B-type conformations in the presence of the [$(Chro)_2-Fe^{II}$] complex, except the duplex containing the GGCC sequence, which exhibited the features of both A- and B-type DNA. In DNA-cleavage assays, the [$(Chro)_2-Fe^{II}$] complex was shown to cause single-stranded cleavage of plasmid DNA because of a Fenton-type reaction. DNA cleavage activity of the [$(Chro)_2-Fe^{II}$] complex was increased at low pH. Moreover, the complex was capable of inhibiting TopI activity. The [$(Chro)_2-Fe^{II}$] complex exhibited higher cytotoxicity than the [$(Mith)_2-Fe^{II}$] complex in several cancer cell lines, most likely owing to its more stable dimeric structure and higher DNA-binding affinity. Our results provide significant evidence that the [$(Chro)_2-Fe^{II}$] complex could be promising in terms of its biological applications in the future.

Both anticancer antibiotics, chromomycin A_3 (Chro)[1] and mithramycin (Mith), are members of the aureolic family isolated from *Streptomyces griseus* and *Streptomyces argillaceus*, respectively (*1–3*). These drugs contain di- and trisaccharide moieties connected to an aglycon chromophore via opposite O-glycosidic bonds, with the A−B disaccharide being on one side, while the C−D−E trisaccharide on the other side (Figure 1A). Their antitumor properties were ascribed to the inhibitory effects of the drugs on replication and transcription during macromolecular biosynthesis (*4*). In addition, both drugs were shown to be powerful inducers of erythroid differentiation of K562 cells and were found to inhibit neuronal apoptosis induced by oxidative stress (*5, 6*).

According to earlier optical spectroscopic analyses, Chro and Mith formed a dimer mediated by a single divalent metal ion, such as Mg^{II} (*7, 8*). The ion-coordinated drug dimer was bound to a DNA duplex around the G/C-rich sequences that were at least three base pairs long (*7, 9*). The solution structures of these two drugs bound to DNA duplexes were analyzed by nuclear magnetic resonance (NMR) spectroscopy, and the crystal structure of the Chro−DNA complex has already been reported (*10–15*). The structures of the Chro−DNA and Mith−DNA complexes show global similarities but with obvious differences in local areas (*16*). It was therefore believed that the differences in the saccharide moieties between Chro and Mith provide the different DNA-binding properties of these two drugs (*17*).

The effects of metal ion alteration leading to amplify the potential of the aureolic family drugs in disease therapy have been discussed (*16, 18*). Previous results reported that Chro is capable of forming a dimeric complex via chelation with metal(II) ions in the absence of DNA (*7*). Binding of Chro to DNA can be achieved only by using metal cations whose ionic radii (less than 85 pm) and charge (+2) were

† This work was supported by the NCS 95-2311-B-005-015-MY2 (to M.-H.H.).

* To whom correspondence should be addressed: Biotechnology Center, National Chung Hsing University, Taichung, 402 Taiwan. Telephone: 886-4-22840450, ext. 6131. Fax: 886-4-22861905. E-mail: mhho@dragon.nchu.edu.tw.

‡ Biotechnology Center, National Chung Hsing University.

§ Institute of Bioinformatics, National Chung Hsing University.

|| Department of Life Science, National Chung Hsing University.

⊥ Department of Biotechnology, Ming Chuan University.

[1] Abbreviation: Chro, chromomycin A_3; Mith, mithramycin; CD, circular dichroism; UV, ultraviolet; SPR, surface plasmon resonance; K_a, association equilibrium constant; K_d, dissociation equilibrium constant; k_a, association rate constant; k_d, dissociation rate constant; TopI, topoisomerase I; CPH, chromophore.

10.1021/bi701915f CCC: $40.75
Published on Web 04/22/2008

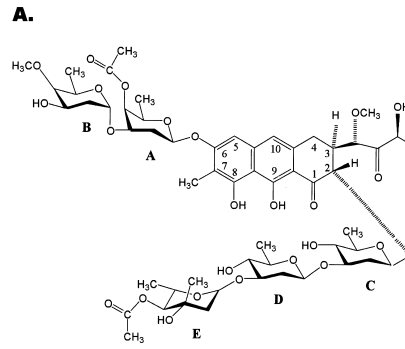

B.

TTTGGCCAAAT G TTTAGCTAAAT G
AAACCGGTTTT AAATCGATTTT

TTTCGCGAAAT G TTTACGTAAAT G
AAAGCGCTTTT AAATGCATTTT

TTTGCGCAAAT G TTTTGCAAAAT G
AAACGCGTTTT AAAACGTTTTT

TTTCCGGAAAT G TTTTCGAAAAT G
AAAGGCCTTTT AAAAGCTTTTT

FIGURE 1: (A) Chemical structure of Chro. (B) Hairpin DNA duplexes with various central tetranucleotides (underlined portions) that were used in this study. In the text, each duplex was named according to the central tetranucleotides contained in the DNA sequence of the duplex, e.g., GGCC, CGCG, GCGC, CCGG, AGCT, ACGT, TGCA, and TCGA.

simultaneously satisfied (*19*). Fe^{II} with an ionic radius of 75 pm shows the highest binding affinity toward Mith among the metal ions, including Mg^{II}, Co^{II}, Ni^{II}, and Zn^{II} (*16*). Our current research has been focused on the studies of the binding of Chro to Fe^{II} as well as mechanisms of the [$(Chro)_2$−Fe^{II}] complex acting on DNA, such as sequence specificity, DNA cleavage, and topoisomerase I (TopI) inhibition. In this study, we found that Chro exhibited higher Fe^{II}-binding affinity compared to Mith. The eight hairpin duplexes with central 5′-GC-3′ and 5′-CG-3′ flanked by G/C or A/T were synthesized and used in the DNA-sequence-specificity study, as shown in Figure 1B. Our results showed that the [$(Chro)_2$−Fe^{II}] complex exhibited strong GC sequence specificity and bound DNA more strongly than the [$(Mith)_2$−Fe^{II}] complex studied previously (*16*). In DNA-cleavage analysis, the effects of different concentrations, time course, and pH values on the cleavage activity of the [$(Chro)_2$−Fe^{II}] complex were explored. Moreover, TopI, the molecular target of a variety of anticancer compounds, could be inhibited by the [$(Chro)_2$−Fe^{II}] complex. Finally, the cytotoxicity of the [$(Chro)_2$−Fe^{II}] complex on several cancer cell lines was also evaluated in this study.

EXPERIMENTAL PROCEDURES

The synthetic DNA oligonucleotides were purified by gel electrophoresis. Chro was purchased from Sigma Chemical Co. (St. Louis, MO). Absorbance measurements were carried out in a quartz cuvette using a Hitachi U-2000 spectrophotometer. The concentrations of Chro were estimated using extinction coefficients of 8800 M^{-1} cm^{-1} at 405 nm (*20*). The concentrations of oligonucleotides were determined according to Beer's law ($A = \epsilon bc$, where A is the optical density at 260 nm, ϵ is the extinction coefficient, b is the cell path length of 1 cm, and c is the DNA concentration in molarity). The extinction coefficient of plasmid DNA is 6600 M^{-1} cm^{-1}. Oligomer extinction coefficients were calculated according to tabulated values of the monomer and dimer extinction coefficients with reasonable assumption (*21*).

Circular Dichroism (CD) Experiments. The CD spectra were collected between 520 and 200 nm with the bandwidth at a 1 nm interval using a JASCO-720 CD spectropolarimeter. All spectra were the average of three runs. Methods of CD spectral analysis were described previously (*22*). The data corresponding to the titration of Chro with divalent metal ions, metal(II) (normalized intensity change at λ_{275} versus metal concentrations), were fitted using a nonlinear least-squares plot. The evaluation of the dissociation equilibrium constant (K_d) between Chro and metal(II) is measured and described as follows:

$$2\text{Chro} + \text{metal(II)} \leftrightarrow (\text{Chro})_2 - \text{metal(II)}$$

At equilibrium, the law of mass action gives

$$K_d = [\text{Chro}]^2[\text{metal(II)}]/[(\text{Chro})_2 - \text{metal(II)}]$$

The CD intensity change (I) of the Chro at λ_{275} can be written as

$$I = I_{max} \times 2[(\text{Chro})_2 - \text{metal(II)}]/[\text{Chro}]_0$$

where $[\text{Chro}]_0$ is the initial Chro concentration and I_{max} is maximum CD intensity change at λ_{275} corresponding to 100% of the complex in solution. At equilibrium, the concentrations in molarity (M) of both Chro and metals in solution can be expressed as

$$[\text{Chro}] = [\text{Chro}]_0 - 2[(\text{Chro})_2 - \text{metal(II)}]$$
$$[\text{metal}] = [\text{metal}]_i - [(\text{Chro})_2 - \text{metal(II)}]$$

where $[\text{metal}]_i$ is the concentration of added metal ion(II) in the solution. Therefore, the unit of K_d is M^2.

Surface Plasmon Resonance (SPR)-Binding Analysis. The affinity, association, and dissociation between drug and DNA duplexes were measured in a BIAcore 3000A SPR instrument (Pharmacia, Uppsala, Sweden) with a SensorChip SA5 from Pharmacia by monitoring the refractive index change of the sensor chip surface. These changes are generally assumed to be proportional to the mass of the molecules bound to the chip and recorded in resonance unit (RU). The 5′-biotin-labeled hairpin DNA duplexes (Figure 1B) purified by polyacrylamide gel electrophoresis (PAGE) were used in SPR experiments. To control the amount of the DNA bound to the SA chip surface, the biotinated oligomer was immobilized manually onto the surface of a streptavidin chip. The metal derivative complex of Chro and 30 mM Tris-HCl buffered solution at a pH of 7.3 in the presence of 50 mM NaCl were prepared and used. Different concentrations of complexes were passed over the chip surface for 180 s at a flow rate of 10 μL min^{-1} to reach the equilibrium, and one of the flow cells was kept blank as a control. The blank buffer solution was then passed over the chip to initiate the dissociation reaction, and this was continued for an additional 300 s to complete the reaction. The surface was then recovered by washing with 10 mM HCl of 10 μL. Analysis of the SPR-binding constant was described previously (*23*). As expected, no response was observed when Chro alone

was run onto the DNA. Sensorgrams for the interactions between hairpin DNA duplex and drug were analyzed using BIA evaluation software of version 3.

Measurement of Breaking the DNA Strand Using Plasmid. *Escherichia coli* was transformed with plasmid DNA, pGEM-7Zf(−), and grown in LB medium. The plasmid DNA was then purified using Qiagen plasmid purification kit (Valencia, CA). Reagents were added in the following order: phosphate buffer at a pH of 7.3, Fe^{II} (or the [(Chro)$_2$−Fe^{II}] complex), supercoiled plasmid DNA, and H_2O_2 (or without H_2O_2). Notice that phosphate buffer instead of Tris was used in the analysis of DNA-strand breakage because Tris was previously shown to generate formaldehyde upon the reaction with hydroxyl radical (*24*). Samples were incubated at 37 °C for 20 min, and the reactions were stopped by thiourea prior to electrophoresis in a 1% agarose gel, followed by ethidium bromide staining for analysis. Quantification of the DNA bands on the gel was achieved using the Uniphoto Band Tool software.

TopI Assays. Binding of the drug complexes to DNA results in the activity inhibition of TopI, which converts DNA from the supercoiled form to an open circular one. In these experiments, 4 μL of assay buffer [35 mmol/L Tris-HCl, 72 mmol/L KCl, 5 mmol/L $MgCl_2$, 5 mmol/L dithiothreitol (DTT), and 5 mM spermidine (pH 7.5)] containing 0.25 μg of pGEM-7Zf(−) was added to tubes prechilled on ice. The drug complex (1, 2.5, 5, 10, and 15 μM) and calf thymus TopI (1 unit; TaKaRa) were added together in a final volume of 10 μL and incubated at 37 °C for 30 min.

Cell Viability. All cell lines were provided from the American Type Culture Collection (Rockville, MD). The human K562 erythroleukemia cell lines were grown in RPMI-1640 supplemented with 10% fetal bovine serum, glucose, L-glutamine, and antibiotics. The other cell lines including the human hepatoblastoma cell lines (HepG2 and Hep3B) and the human breast cancer cell line (MCF-7) were grown in Dulbecco's modified Eagle medium (DMEM) containing the same supplements as those described for RPMI-1640. All cells were maintained in a 5% CO_2 atmosphere at 37 °C. Cellular proliferations were evaluated using the WST kit assay (Roche). Because of its high efficiency, the WST assay is a better colorimetric assay compared to the MTT assay. The assay is based on the ability of viable cells to reduce a soluble yellow tetrazolium salt (WST) to dark red formazan crystals. The cells were seeded into 96-well plates. The drug complexes were dissolved in the medium described above and added to the cell solutions over a range of concentrations (0–10 μM). Treatment of cell lines for 48 h with 10 μM $FeCl_2$ alone did not apparently influence the cell viability. After 24–48 h, WST dye of 10 μL was added and the plates were incubated in a moist chamber at 37 °C for an additional 3 h. Optical density was measured at 470 nm in an ELISA reader. At least three independent experiments were performed to obtain the results for statistical analysis.

RESULTS

Interactions of Chro with Fe^{II}. The conformational change of Chro upon binding to Fe^{II} was characterized using CD spectroscopy. As shown in Figure 2, the CD spectra of Chro were scanned from 200 to 520 nm in the presence of increasing concentrations (0.00–0.10 mM) of Fe^{II}. The spectral features in the 250–300 nm most likely arose from the absorption assigned to the aglycon chromophore ring of Chro that was polarized along the long axis based on the studies of Mith (*25, 26*). The occurrence of one isosbestic point at 285 nm remaining basically unchanged demonstrates the presence of one-mode conformation alteration of Chro upon binding to Fe^{II}. The CD spectral peaks of Chro were distinctly inverted in the 250–300 nm region when the concentration of Fe^{II} was above 0.02 mM. The results presented here clearly show that a strong interaction exists between Chro and Fe^{II} because the electronic transition of Chro chromophore was changed, possibly owing to the coordination of Fe^{II} with the oxygen atoms of each chromophore ring of Chro. The dimer dissociation constant, K_d (in M^2), between Chro and Fe^{II} was calculated to be 6.80×10^{-12}. The result showed that Chro exhibits the highest binding affinity toward Fe^{II}, as shown by its lowest K_d, by forming a dimeric complex, compared to Mith with K_d being 5.03×10^{-11} (*16*).

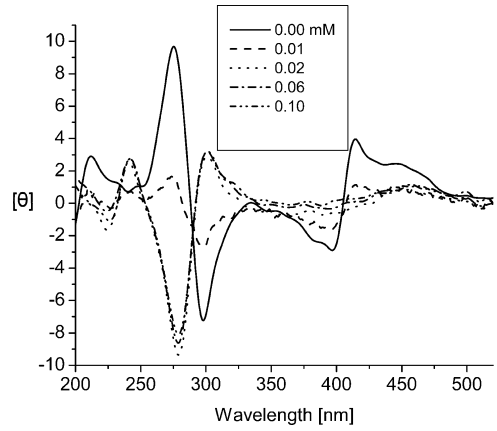

FIGURE 2: CD spectra of Chro in the presence of Fe^{II} with the concentration varying from 0 to 0.1 mM (bottom) at 25 °C. The drug concentration is 0.04 mM, buffered by 20 mM Tris-HCl at a pH of 7.3. The one isobestic point at 285 nm remains basically unchanged of Chro association with the Fe^{II} ion.

Interactions of the [(Chro)$_2$−Fe^{II}] Complex with Hairpin DNA Duplexes Using SPR. To characterize the binding modes between the [(Chro)$_2$−Fe^{II}] complex and DNA, the [(Chro)$_2$−Fe^{II}] complex was allowed to interact with biotin-labeled hairpin DNA duplexes and the results were monitored by SPR. The DNA tested here form self-complementary hairpin duplexes by using trinucleotides, 5′-TGT-3′, as a loop region. In addition, their stem regions were identical, except for the central portion of four paired nucleotides that have central 2 base-paired (bp) G-tract with directions of either 5′-GC-3′ or 5′-CG-3′ flanked by G and C, i.e., 4 bp G-tract (or A and T, i.e., 2 bp G-tract flanked by A and T). In Figure 3, the association between hairpin DNA duplexes and the [(Chro)$_2$−Fe^{II}] complex was shown by increased levels of RU values, whereas the dissociation between these two species was noticed by a sharp drop in the RU values on the same trace. According to the SPR sensorgram, the interactions between GGCC and the [(Chro)$_2$−Fe^{II}] complex and between TCGA and the [(Chro)$_2$−Fe^{II}] complex showed the highest maximum (∼290 RU) and the lowest minimum (∼50 RU) binding capacities, respectively.

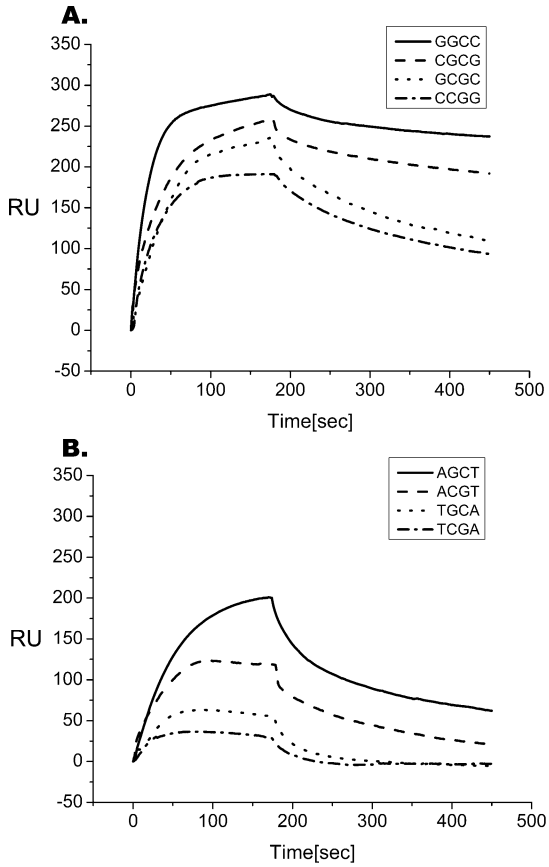

FIGURE 3: (A and B) SPR sensorgram of the Chro−DNA interaction between immobilized hairpin duplex and the target [$(Chro)_2$−Fe^{II}] complex. The concentration of each target was 5 μM, in 50 mM NaCl, buffered by 25 mM Tris-HCl at pH 7.3 and 20 °C.

The kinetic constants for association (k_a in M^{-1} s^{-1}) and dissociation (k_d in s^{-1}) of the [$(Chro)_2$−Fe^{II}] complex binding to hairpin DNA duplexes are shown in parts A and B of Figure 4 based on the calculation from the association and dissociation phases of SPR traces, respectively. In the duplexes containing regions of 4 bp G-tract, GGCC exhibited the highest k_a, 2.66×10^3 M^{-1} s^{-1}, followed by CGCG of k_a, 2.24×10^3 M^{-1} s^{-1}. The k_a values were essentially the same, 2.15×10^3 and 2.17×10^3 M^{-1} s^{-1}, for GCGC and CCGG, respectively. The other duplexes containing regions of 2 bp G-tract flanked by A and T (AGCT, ACGT, TGCA, and TCGA) were shown to have lower k_a values, compared to those containing regions of 4 bp G-tract as shown in Figure 4A. AGCT and ACGT showed approximately the same k_a, 1.65×10^3 and 1.68×10^3 M^{-1} s^{-1}, upon binding to the [$(Chro)_2$−Fe^{II}] complex, respectively. TGCA and TCGA showed much lower k_a, 7.54×10^2 and 5.63×10^2 M^{-1} s^{-1}, respectively, in this study. As for the dissociation rate constants, GGCC showed the lowest k_d, 8.76×10^{-4} s^{-1}, compared to any other duplexes examined in this study, followed by CGCG, with its k_d being 1.42×10^{-3} s^{-1}. The k_d of GCGC and CCGG were basically the same, 3.70×10^{-3} and 3.55×10^{-3} s^{-1}, respectively, and higher than the k_d of GGCC and CGCG. The k_d, 5.63×10^{-3} and 6.91×10^{-3} s^{-1}, of AGCT and ACGT, respectively, were increasingly higher, and they were all slightly above the k_d of GCGC and CCGG. However, TGCA and, especially, TCGA were found to exhibit much higher k_d as shown in Figure 4B.

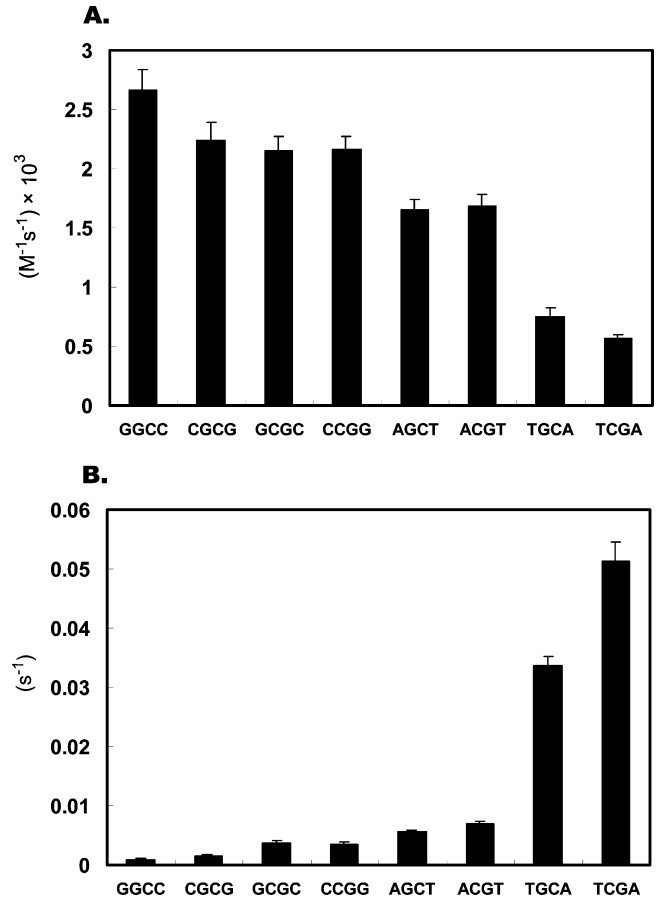

FIGURE 4: (A) k_a and (B) k_d values derived from the DNA-target-binding sensorgrams between immobilized hairpin duplex and the target [$(Chro)_2$−Fe^{II}] complex. All binding experiments were completed with at least three different concentrations for each target strand. The methods for determining k_a and k_d are described in the Experimental Procedures.

Table 1: Association Equilibrium Constants (K_a) between the [$(Chro)_2$−Fe^{II}] Complex and the Hairpin Duplexes

duplexes	K_a $(M^{-1})^a$	duplexes	K_a $(M^{-1})^a$
GGCC	$3.03 \pm 0.28 \times 10^6$	AGCT	$2.93 \pm 0.22 \times 10^5$
CGCG	$1.57 \pm 0.14 \times 10^6$	ACGT	$2.43 \pm 0.15 \times 10^5$
GCGC	$5.80 \pm 0.45 \times 10^5$	TGCA	$2.21 \pm 0.18 \times 10^4$
CCGG	$6.19 \pm 0.52 \times 10^5$	TCGA	$1.11 \pm 0.10 \times 10^4$

[a] K_a values obtained from k_a divided by k_d.

The association constants (K_a) of all hairpin DNA duplexes upon binding to the [$(Chro)_2$−Fe^{II}] complex were calculated as k_a/k_d (in M^{-1}) and listed in Table 1. As expected, GGCC showed the highest K_a, approximately twice the K_a of CGCG, whereas GCGC and CCGG exhibited the lowest K_a, among all of the duplexes containing regions of 4 bp G-tract studied here. As for duplexes containing regions of 2 bp G-tract flanked by A and T, their K_a values were all lower than those containing 4 bp G-tract, suggesting that hairpin DNA duplexes containing regions of 4 bp G-tract tend to interact with the [$(Chro)_2$−Fe^{II}] complex more strongly and in a sequence-specific manner, compared to those duplexes such as the ones containing regions of 2 bp flanked by A and T under the current study. In addition, the calculation of k_d appears to be more crucial in terms of the determination of binding constants. The association constant of the [$(Mith)_2$−Fe^{II}] complex bound to GGCC has also been evaluated by SPR. Our studies showed here that the

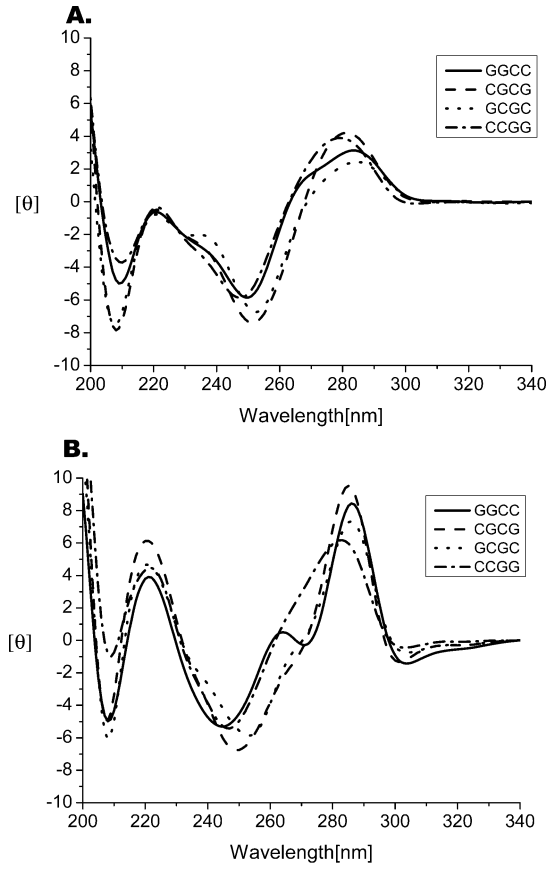

FIGURE 5: (A) CD spectra of hairpin DNA duplexes including GGCC, CGCG, GCGC, and CCGG in 25 mM Tris-HCl buffer at pH 7.3 with 50 mM NaCl at 25 °C. The concentration of DNA was 20 μM. (B) Normalized sum of the CD specta of the [(Chro)$_2$−Fe^{II}]−hairpin DNA duplex including GGCC, CGCG, GCGC, and CCGG minus [(Chro)$_2$−Fe^{II}] dimer in 25 mM Tris-HCl buffer at pH 7.3 with 50 mM NaCl at 25 °C.

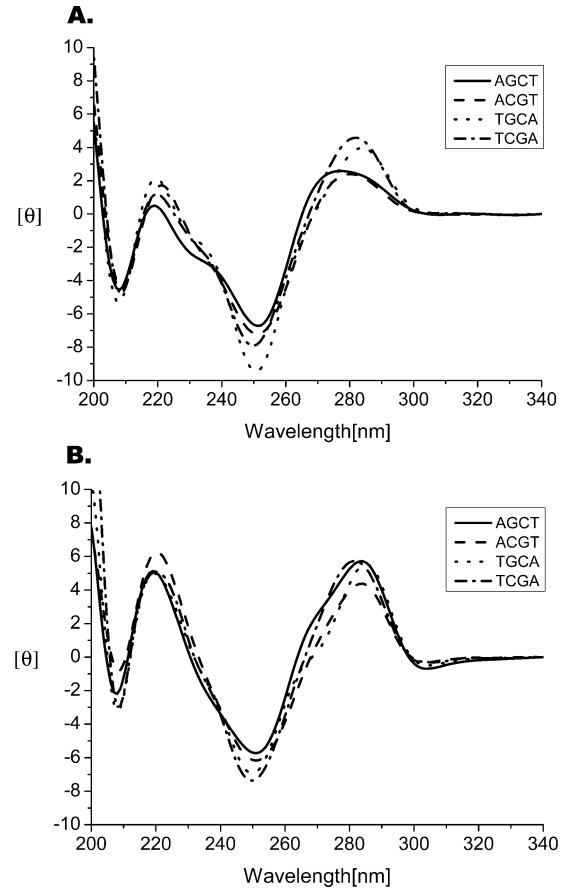

FIGURE 6: (A) CD spectra of hairpin DNA duplexes including AGCT, ACGT, TGCA, and TCGA. The concentration of DNA was 20 μM. (B) Normalized sum of the CD spectrum of the [(Chro)$_2$−Fe^{II}]−hairpin DNA duplex including AGCT, ACGT, TGCA, and TCGA minus [(Chro)$_2$−Fe^{II}] dimer in 25 mM Tris-HCl buffer at pH 7.3 with 50 mM NaCl at 25 °C.

[(Chro)$_2$−Fe^{II}] complex exhibits 6-fold DNA-binding affinity higher, compared to the [(Mith)$_2$−Fe^{II}] complex studied previously (*16*).

Effects of the [(Chro)$_2$−Fe^{II}] Complex on the Conformations of Hairpin DNA Duplexes. To explore the conformational changes of hairpin DNA duplexes upon binding to the [(Chro)$_2$−Fe^{II}] complex, DNA conformations were monitored in the absence or presence of the [(Chro)$_2$−Fe^{II}] complex using CD spectroscopy. Previously, we showed that the conformation of [(Chro)$_2$−Mg^{II}] remains basically unchanged with and without DNA (*15*). Therefore, in the CD spectra of hairpin DNA duplexes complexed to [(Chro)$_2$−Fe^{II}], the CD spectra of the [(Chro)$_2$−Fe^{II}] complex were all subtracted to minimize the interference from [(Chro)$_2$−Fe^{II}]. In Figure 5A, the CD spectra of the hairpin DNA duplexes containing regions of 4 bp G-tract showed the same profiles, i.e., their CD spectra showed a band of negative and positive peak at 250 and 280 nm, typical of B-DNA, respectively (*22, 23*). After binding to the [(Chro)$_2$−Fe^{II}] complex, all hairpin DNA duplexes containing regions of 4 bp G-tract showed an increase in the intensity of their CD spectra at ∼220 and 280 nm (Figure 5B). It is interesting to note that GGCC was shown to exhibit the largest change in its CD intensity at 280 nm, and a smaller peak arising at 265 nm, characteristic of the CD spectra of A-DNA, was noticed in the presence of the [(Chro)$_2$−Fe^{II}] complex.

The interactions between hairpin DNA duplexes containing regions of 2 bp G-tract flanked by A and T and [(Chro)$_2$−Fe^{II}] were also studied using CD spectroscopy in a similar manner. Unlike those duplexes containing regions of 4 bp G-tract, the interactions between these duplexes and [(Chro)$_2$−Fe^{II}] were shown to increase only to a limited extent as shown by the peak heights at ∼220 and 280 nm (parts A and B of Figure 6). This is basically consistent with the observation that hairpin DNA duplexes containing regions of 2 bp G-tract flanked by A and T exhibited lower equilibrium constants, K_a, upon binding to [(Chro)$_2$−Fe^{II}]. In addition, the CD spectra of AGCT and ACGT were shown to shift to longer wavelengths (∼275−280 nm), suggesting a slightly different binding mode that exists for these two duplexes to accommodate the incoming [(Chro)$_2$−Fe^{II}]. These red shifts were not observed in TGCA and TCGA of the same category, however.

Effects of the [(Chro)$_2$−Fe^{II}] Complex on DNA Cleavage in Plasmid DNA. DNA cleavage converts the supercoiled form of plasmid DNA into relaxed open circular and linear forms by one- and two-strand cleavages, respectively. To study the DNA cleavage activity of the [(Chro)$_2$−Fe^{II}] complex, plasmid DNA, pGEM-7zf(−), was treated with [(Chro)$_2$−Fe^{II}] in the absence or presence of H_2O_2. The DNA cleavage activity of the [(Chro)$_2$−Fe^{II}] complex was examined according to the levels of plasmid DNA integrity at physiological pH. Untreated supercoiled plasmid was ob-

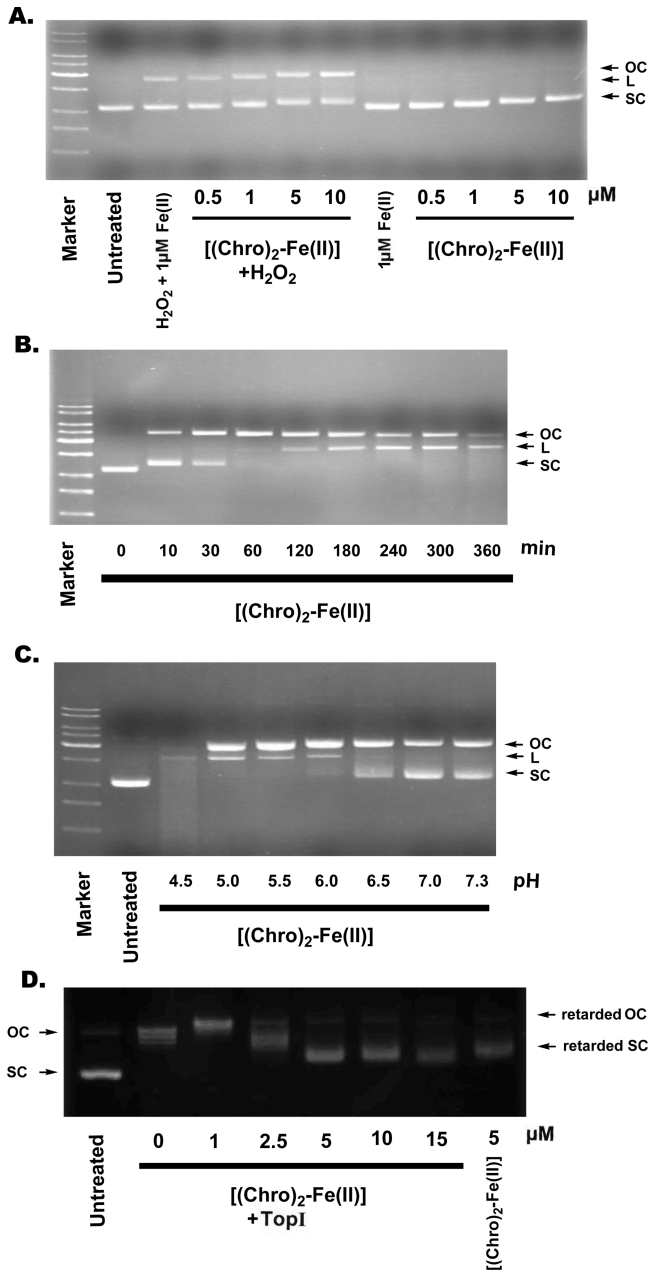

FIGURE 7: (A) Effects of the [$(Chro)_2-Fe^{II}$] complex on the integrity of the supercoiled plasmid DNA when incubated in the absence and presence of hydrogen peroxide. The concentrations of the drug complex are represented as 1, 10, 20, and 40 μM, respectively. (B) Plasmid DNA was treated with [$(Chro)_2-Fe^{II}$] (10 μM) in the presence of H_2O_2 at various time points (0, 10, 30, 60, 120, 180, 240, 300, and 360 min). (C) Plasmid DNA was treated with [$(Chro)_2-Fe^{II}$] (10 μM) in the presence of H_2O_2 at various pH values (4.5–7.3). (D) Effect of the [$(Chro)_2-Fe^{II}$] complex on the TopI activity. In these experiments, 4 μL of assay buffer containing 0.5 μg/mL pGEM-7Zf(−) were added to tubes on ice. The drug complex (1, 2.5, 5, 10, and 15 μM) and TopI (1 unit) were added to a total of 10 μL.

served as a single band on gels. For a comparison, reactions were also carried out with Fe^{II} (1 μM) alone. When plasmid DNA was treated with increasing concentrations of [$(Chro)_2-Fe^{II}$] in the presence of H_2O_2, the levels of plasmid DNA open circular forms caused by relaxation were increased along with the concentrations of [$(Chro)_2-Fe^{II}$] (Figure 7A). On the other hand, however, no plasmid DNA relaxation (cleavage) was observed in the absence of H_2O_2, suggesting that the DNA cleavage activity of [$(Chro)_2-Fe^{II}$] on plasmid DNA was achieved via a Fenton-type reaction. In the time-course experiments, plasmid DNA was treated with [$(Chro)_2-Fe^{II}$] (10 μM) in the presence of H_2O_2 at various time points as shown in Figure 7B. At 60 min, the supercoiled form of plasmid DNA was completely converted into open circular form. Moreover, after 120 min, the level of linear form plasmid DNA caused by [$(Chro)_2-Fe^{II}$] was increased along with time. These results confirmed the observation that plasmid breakage occurs by the formation of double-strand scissions, which results from the stepwise cleavage of single strands (*27*).

The pH value of a solution plays an important role in the radical-mediated DNA damage caused by drug−metal complexes, because it may influence the coordination mode, as well as the oxidative activity, of the complex (*27*). Figure 7C presents the results of plasmid DNA treated with [$(Chro)_2-Fe^{II}$] (10 μM) in the presence of H_2O_2 at various pH values and incubated for 30 min. At physiological pH (7.3), some of the plasmid DNA was relaxed to open circular form DNA. With the decrease in pH, the levels of DNA of both open circular and linear forms were increased. At pH 4.5, supercoiled DNA destruction is almost complete, as shown by the appearance of the smear of shorter DNA fragments. Moreover, the slight retardation of DNA at a pH range (4.5–5.5) showed that [$(Chro)_2-Fe^{II}$] exhibits weaker DNA-binding affinity at low pH.

Inhibitory Effects of the [$(Chro)_2-Fe^{II}$] Complex on TopI Activity. It is well-known that TopI acts by cleaving and rejoining of one strand of DNA duplex and leads to relaxation of the supercoiled form DNA. To explore the inhibitory effects of [$(Chro)_2-Fe^{II}$] on the activity of TopI, supercoiled plasmid DNA, pGEM-7zf(−), was treated with TopI in the presence of increasing concentrations of the [$(Chro)_2-Fe^{II}$] complex. As shown in Figure 7D, in the absence of [$(Chro)_2-Fe^{II}$] (0 mM), all of the plasmid was converted into open circular form. However, in the presence of increasing concentrations of the [$(Chro)_2-Fe^{II}$] complex (1–15 μM), the levels of open circular form plasmid were diminished. The DNA relaxation effects caused by TopI were totally inhibited by the [$(Chro)_2-Fe^{II}$] complex at 5 μM. Because the gel mobility of plasmid DNA was slightly retarded at higher concentrations (e.g., 5 μM) of the [$(Chro)_2-Fe^{II}$] complex with the enzyme, it is believed that the DNA-bound [$(Chro)_2-Fe^{II}$] complex expels the TopI from approaching plasmid DNA and in turn leads to a lower level of DNA relaxation.

Cytotoxicity of the [$(Chro)_2-Fe^{II}$] Complex to Different Cancer Cell Lines. Hepatoma, leukemia, and breast cancer have been diagnosed worldwide and caused numerous deaths at high rates (*28*). To evaluate the possibility of the [$(Chro)_2-Fe^{II}$] complex applied in cancer therapy, the cytotoxicity of the [$(Chro)_2-Fe^{II}$] complex in HepG2, Hep3B, K562, and MCF7 cell lines was assessed by the WST assay. The activity was compared to Chro alone as a control. The treatment of both cell lines for 48 h with 10 μM $FeCl_2$ alone did not visibly affect the cell viability. Table 2 shows the GI_{50} values of HepG2, Hep3B, K562, and MCF-7 cells when incubated with Chro at 24 and 48 h in the absence or presence of constant Fe^{II} (5 μM). Hep3B cells appeared to be more sensitive to Chro, as compared to HepG2 cells. However, Fe^{II} was shown to potentiate the antiproliferation effects of Chro to HepG2 at 48 h, with the GI_{50} value being

Table 2: GI$_{50}$[a] (micromolar) of Chro and the [(Chro)$_2$−Fe^{II}] Complex in Various Cancer Cell Lines at 24 and 48 h

cell-line type	Chro (μM)		[(Chro)$_2$−Fe^{II}] (μM)	
	24 h	48 h	24 h	48 h
HepG2	>10	5 (±2)	>10	0.3 (±0.2)
Hep3B	0.5 (±0.1)	0.1 (±0.03)	0.1 (±0.04)	0.1 (±0.01)
K562	1 (±0.5)	0.06 (±0.02)	0.1 (±0.04)	0.05 (±0.02)
MCF-7	>10	0.08 (±0.01)	>10	0.09 (±0.01)

[a] GI$_{50}$ indicates 50% inhibitory concentration of growth.

0.3 μM. These values showed more than 10-fold cytotoxicity compared to those of Chro treatment alone at 48 h. Moreover, Fe^{II} increased the cytotoxicity to Hep3B in response to Chro at 24 h. In addition, we tested the cytotoxicity of the [(Chro)$_2$−Fe^{II}] complex toward other cell lines, including K562 erythroleukemia cells and MCF-7 breast cancer cells under the same conditions as described for HepG2 and Hep3B cell lines. Chro in the presence of Fe^{II} was shown to be more active to K562 cells, with GI$_{50}$ values being 0.1 μM at 24 h, than Chro alone. Although no significant effect after either 24 or 48 h exposure was seen in MCF-7 cancer cells, the [(Chro)$_2$−Fe^{II}] complex maintained its cytotoxicity comparable to free Chro.

DISCUSSION

The dimer of Chro chelated with Fe^{II} can be achieved when Fe^{II} is at low-spin state with an ionic radius of 75 pm (*19, 29*). It is believed that the rigid steric configuration of the bidentate Chro containing two neutral oxygen atoms on the chromophore causes large ligand field splitting on central metal ions and leads to low-spin states of chelated divalent metal ions, except, of course, Mg^{II} and Zn^{II}. The geometry around Fe^{II} is presumably octahedral in the dimeric complex of [(Chro)$_2$−Fe^{II}], in which the unequal population of all six Fe^{II} d electrons completely filling in the low-energy t_{2g} orbitals because of ligand field splitting causes maximal ligand field stabilization energy and therefore leads to the strong interaction between Chro and Fe^{II}. Nevertheless, the spin state of Fe^{II} in the [(Chro)$_2$−Fe^{II}] complex needs to be proven by future experiments using techniques such as low-temperature EPR spectroscopy. Our results showed that Chro was converted into a more stable dimer complex in the presence of Fe^{II} in comparison to Mith. The difference in the saccharide residues between Chro and Mith is most likely the cause that results in the difference of Fe^{II}-binding affinity. When the metalloantibiotics are applied to function as clinical trails, their structural integrity can be destroyed by other species, however. For example, polyamines, e.g., spermine, exist in the nucleus of the cancer cell at millimolar range and have been reported to interact with transition metals, such as Fe^{II} and Cu^{II}, possibly resulting in the interference of the action of DNA-binding metalloantibiotics (*30*). Recently, our findings showed that the more stable dimeric complex of [(Chro)$_2$−Fe^{II}] exhibited stronger structural integrity than [(Mith)$_2$−Fe^{II}] against the competition of spermine toward Fe^{II} according to our CD spectral analyses (unpublished data).

The sequence-specific binding of Chro to DNA in the presence of a high concentration of Mg^{II} has been reported (*31*). Keniry et al. have shown that the 5′-CG base pair step is less favored by Chro compared to the 5′-GC and 5′-GG

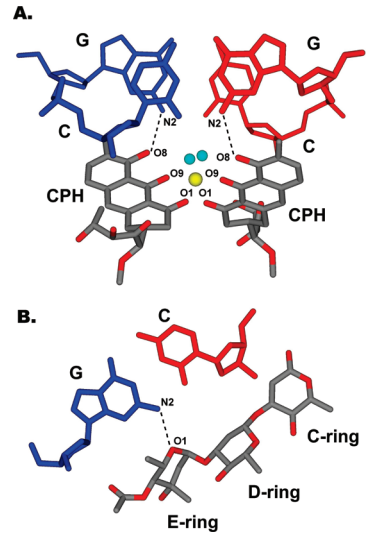

FIGURE 8: (A) Close-up view of the molecular structure of the Chro−DNA complex at the central GC step showing two specific intermolecular hydrogen bonds existing between the O8 of the Chro chromophore (CPH) and the N2 atom of the central 5′-G. Two water molecular and metal(II) ions were represented by light-blue and yellow balls, respectively. (B) Detailed conformation showing the hydrogen bonding between the O1 oxygen of the Chro E ring and the N2 hydrogen atom of flanking guanine bases.

sites according to their NMR studies (*14*). The results by Liu and Chen supported the earlier NMR findings and further revealed that the preference of Chro for the 5′-GC step was significantly modulated by the adjacent base pairs (*31*). In the current study, our SPR results clearly showed that the binding affinity of the [(Chro)$_2$−Fe^{II}] complex to hairpin DNA duplexes follows the order: GGCC > CGCG > CCGG ∼ GCGC > AGCT > ACGT > TGCA > TCGA. The considerably weaker binding of GCGC, CCGG, ACGT, and TCGA each containing a central 5′-CG step, as compared to the corresponding sequence isomers, GGCC, CGCG, AGCT, and TGCA, each containing a central 5′-GC step, suggested that the sequence specificity at the 5′-GC step of the [(Chro)$_2$−Fe^{II}] complex is similar to the [(Chro)$_2$−Mg^{II}] complex. The strong preference for the central 5′-GC step can be explained by two specific intermolecular hydrogen bonds existing between the O8 of Chro chromophore and the N2 atom of central 5′-G (or the corresponding 5′-G in the complementary strand), in addition to the one between O3 of the B-ring side chain and O2P of the same 5′-G (*15*) (Figure 8A). To further understand the kinetic behavior of the [(Chro)$_2$−Fe^{II}] complex bound to DNA, we analyzed the SPR data on the association and dissociation phases between the drug and DNA hairpins with various sequences. The [(Chro)$_2$−Fe^{II}] complex was shown to bind to DNA containing regions of 4 bp G-tract so fast that they reached nearly the same levels of association rates. A widening minor groove is essential for the DNA duplex to allow the [(Chro)$_2$−Fe^{II}] complex access to the minor groove. Earlier studies have shown that DNA containing the sequence of 4 bp G-tract has a propensity to exhibit a wider minor groove (*32*). In addition, the rates of dissociation of the [(Chro)$_2$−Fe^{II}] complex from DNA duplexes were modulated significantly by the adjacent base pairs. For example, despite the presence of an identical central GC step, the [(Chro)$_2$−Fe^{II}] complex dissociates from GGCC slower, compared to CGCG, AGCT, and TGCA. According to the

crystal structure of the Chro−DNA complex, the specific strong intermolecular Chro−DNA hydrogen bonding between the O1 oxygen of E-ring and the N2 hydrogen atom of flanking guanine bases is most likely responsible for this observation (*15*) (Figure 8B). In the DNA minor groove, only purine N3, pyrimidine O2, guanine N2, and deoxyribose O4′ atoms are involved in the interactions with drugs (*33*). Therefore, the decreased binding affinity when the flanking 5′-guanine is replaced by cytosine can be explained by a different redirected orientation of the hydrogen bonding originally formed between the O1 of the E ring and the N2 atom of the flanking guanine to a less favorable direction. In the cases where the central 5′-GC were flanked by A and T, the O1 of the E ring completely lacks the possibility to form a hydrogen bond in the minor groove. Furthermore, in the duplex of TGCA, the O2 atom of thymine creates a steric repulsion against the O1 of the E ring, which explains the lowest binding affinity of the duplex containing central TGCA toward [$(Chro)_2$−Fe^{II}], compared to other duplexes under the same conditions.

Transcription factors, e.g., Sp1, bound to GC-rich sequences in promoter regions are associated with cancer pathogenesis (*34*). Blocking the binding of transcription factors to DNA by DNA-binding drugs and in turn modulating gene expression have become attractive issues in cancer therapy (*34*). Wu et al. reported that hedamycin, a GC-rich sequence-specific DNA-binding drug, enhanced apoptosis of tumor cells by binding to a GC-rich element in the core promoter region and denied the accessibility of this sequence to Sp1 or Sp1-like proteins involved in antiapoptotic protein transcription (*35*). Mith has also been identified to show the ability to downregulate the expression of many cancer-related genes by blocking the binding of Sp1 to the P1 promoter region (*36, 37*). As a consequence of our SPR results showing GC sequence specificity exhibited by the [$(Chro)_2$−Fe^{II}] complex, this drug complex has the potential to inhibit the gene transcription regulated by these factors.

Previous NMR structural studies indicated that Chro induces a conformational change in the nucleotide from a B-like helix conformation to the one that has A-like characteristics at some segments of the sequence (*13, 14*). However, our X-ray crystallographic studies showed that the DNA structure of the Chro−DNA complex maintained a right-handed helical structure, with the central 4 bp segment adopting a B-like character with a pronounced kink (*15*). In the present CD study, the hairpin DNA duplexes containing 2 and 4 bp G-tracts used here exhibited B-DNA CD profiles in the absence of the [$(Chro)_2$−Fe^{II}] complex. Previous CD and Fourier transform infrared spectroscopy (FTIR) studies concluded that the structures of the G-tracts in solution are all in a dominant B-type conformation (*38*). In addition, the decamer d(CATGGCCATG) with a 4 bp G-tract has also been shown to crystallize as B-DNA (*39*). The CD spectral intensity change of DNA was increased by the [$(Chro)_2$−Fe^{II}] complex, but no significant variation in the spectral features for DNA structure was noticed in CD spectra. What was particularly noticeable is that the [$(Chro)_2$−Fe^{II}] complex increased the intensity of the CD spectrum at 280 and 265 nm arising in the GGCC and suggests that an unusual structure of GGCC caused by the drug complex has the characteristics of both A- and B-type organization of bases in the helices. Besides GGCC, the other hairpin DNA duplexes in the presence of the [$(Chro)_2$−Fe^{II}] complex seem to retain the same DNA type, i.e., B-type conformation.

Several DNA-binding anticancer compounds, such as bleomycin, that facilitate the redox reactions of metal ions including Fe^{II} and Co^{III}, which generate damaging hydroxyl radicals to cause DNA stand breaks, are able to kill cancer cells (*40*). The present study provides strong evidence that the [$(Chro)_2$−Fe^{II}] complex can promote single-stranded breakage of plasmid DNA in the presence of hydrogen peroxide via a Fenton-type reaction. Additionally, DNA characteristic ladders of the internucleosomal DNA cleavage that occurred during treatment of the [$(Chro)_2$−Fe^{II}] complex were also observed by agarose gel electrophoresis of DNA isolated from hepatoma cancer cell lines (Figure S1 in the Supporting Information). At low pH, the [$(Chro)_2$−Fe^{II}] complex showed higher oxidative activity, while the complex displays relatively low DNA-binding affinities. Our results are consistent with what was observed by Tadolini and Carbrini; i.e., hydroxyl radical damage to deoxyribose is more pronounced at acidic pH compared to neutral and moderately basic pH (*41*). Besides, it was previously shown that iron catalytically decomposes H_2O_2 into oxygen and water at high pH without forming hydroxyl radicals (*42*). This explains why the [$(Chro)_2$−Fe^{II}] complex exhibits lower DNA cleavage activity at physiological conditions.

DNA topoisomerases, which solve topological problems created by the double-helical structure of DNA in essential cellular processes, are the targets of many therapeutic agents (*43, 44*). Various topoisomerase inhibitors, particularly, camptothecins and its analogue, the so-called topoisomerase poisons, are drugs presently used in cancer therapy (*45*). They inhibit TopI activity by trapping a reversible TopI−DNA cleavable complex (*46*). Two problems arising limit their use in clinical trails, however (*46, 47*). First, they rapidly diffuse from the TopI−DNA complex and must be given as a prolonged infusion to maintain persistent cleavage complexes long enough to be converted into DNA damage. Second, TopI is the only target of these poisons, and several tumors have become resistant to these drugs, which leads to declined antitumor activity when applied to cancer patients. A search for other types of drugs that act on the same target, TopI, but by different modes of action is needed (*43*). Previously, a series of novel anticancer drugs, such as thiazole-containing oligopeptides interacting specifically with the minor groove of DNA, was also shown to inhibit TopI (*48*). Our study showed that at low concentrations, the [$(Chro)_2$−Fe^{II}] complex was able to inhibit the activity of TopI, as shown by the conversion of supercoiled DNA to the open circular one. Unlike real topoisomerase poisons, which trap covalent complexes between enzymes and DNA, the [$(Chro)_2$−Fe^{II}] complex interfered with the action of topoisomerase most likely via minor-groove binding. However, the real mechanism of TopI inhibition caused by the [$(Chro)_2$−Fe^{II}] complex remains to be elucidated.

A large number of potent symmetrical cytotoxic agents that act by different mechanisms have been investigated (*49*). Our current study suggests that the [$(Chro)_2$−Fe^{II}] complex acts on DNA in a diverse way. In comparison of the cytotoxicity between the [$(Chro)_2$−Fe^{II}] complex and the [$(Mith)_2$−Fe^{II}] complex, our studies concluded that Chro in the presence of Fe^{II} showed potential antitumor activities more than that of the [$(Mith)_2$−Fe^{II}] complex because of its

stable dimeric structure and higher DNA-binding affinity. Many studies using cell culture, animal models, and clinical trials have shown that some anticancer drugs, including cisplatin, bleomycin, or doxorubicin, are known to interact with DNA duplexes before exerting their biological activities. The search of strategies for selectively inhibiting cancer cell growth is vital, given the fact that some tumors may become resistant to conventional chemotherapy, which leads to declined antitumor activity of drugs applied to cancer patients. In summary, our results may provide important insights into the properties of Chro chelated with iron(II) to generate a stable dimeric complex that may be applied to biological application in the future.

ACKNOWLEDGMENT

We thank Dr. Andrew H.-J. Wang and L. S. Kan (Academia Sinica) for their helpful resource that made this research possible. We also thank Y. C. Lo (Yang-Ming University) for his assistance in topoisomerase assay.

SUPPORTING INFORMATION AVAILABLE

DNA characteristic ladders of the internucleosomal DNA cleavage that occurred during treatment of the [$(Chro)_2$−Fe^{II}] complex, observed by agarose gel electrophoresis of DNA isolated from hepatoma cancer cell lines (Figure S1). This material is available free of charge via the Internet at http://pubs.acs.org.

REFERENCES

1. Du Priest, R. W., Jr., and Fletcher, W. S. (1973) Chemotherapy of testicular germinal tumors. *Oncology 28*, 147–163.
2. Slavik, M., and Carter, S. K. (1975) Chromomycin A_3, mithramycin, and olivomycin: Antitumor antibiotics of related structure. *Adv. Pharmacol. Chemother. 12*, 1–30.
3. Foley, J. F., Lemon, H. M., Miller, D. M., and Kessinger, A. (1972) The treatment of metastatic testicular tumors. *J. Urol. 108*, 439–442.
4. Ming, L. J. (2003) Structure and function of "metalloantibiotics". *Med. Res. Rev. 23*, 697–762.
5. Chatterjee, S., Zaman, K., Ryu, H., Conforto, A., and Ratan, R. R. (2001) Sequence-selective DNA binding drugs mithramycin A and chromomycin A_3 are potent inhibitors of neuronal apoptosis induced by oxidative stress and DNA damage in cortical neurons. *Ann. Neurol. 49*, 345–354.
6. Bianchi, N., Osti, F., Rutigliano, C., Corradini, F. G., Borsetti, E., Tomassetti, M., Mischiati, C., Feriotto, G., and Gambari, R. (1999) The DNA-binding drugs mithramycin and chromomycin are powerful inducers of erythroid differentiation of human K562 cells. *Br. J. Hamaetol. 104*, 258–265.
7. Aich, P., Sen, R., and Dasgupta, D. (1992) Role of magnesium ion in the interaction between chromomycin A_3 and DNA: Binding of chromomycin A_3−Mg^{2+} complexes with DNA. *Biochemistry 31*, 2988–2997.
8. Aich, P., and Dasgupta, D. (1990) Role of Mg^{+2} in the mithramycin−DNA interaction: Evidence for two types of mithramycin−Mg^{+2} complex. *Biochem. Biophys. Res. Commun. 173*, 689–696.
9. Chakrabarti, S., Aich, P., Sarker, D., Bhattacharyya, D., and Dasgupta, D. (2000) Role of Mg^{2+} in the interaction of anticancer antibiotic, chromomycin A_3 with DNA: Does neutral antibiotic bind DNA in absence of the metal ion? *J. Biomol. Struct. Dyn. 18*, 209–218.
10. Sastry, M., and Patel, D. J. (1993) Solution structure of the mithramycin dimer−DNA complex. *Biochemistry 32*, 6588–6604.
11. Sastry, M., Fiala, R., and Patel, D. J. (1995) Solution structure of mithramycin dimers bound to partially overlapping sites on DNA. *J. Mol. Biol. 251*, 674–689.
12. Gochin, M. (2000) A high-resolution structure of a DNA−chromomycin−Co(II) complex determined from pseudocontact shifts in nuclear magnetic resonance. *Struct. Fold Des. 8*, 441–452.
13. Gao, X. L., Mirau, P., and Patel, D. J. (1992) Structure refinement of the chromomycin dimer−DNA oligomer complex in solution. *J. Mol. Biol. 223*, 259–279.
14. Keniry, M. A., Banville, D. L., Simmonds, P. M., and Shafer, R. (1993) Nuclear magnetic resonance comparison of the binding sites of mithramycin and chromomycin on the self-complementary oligonucleotide $d(ACCCGGGT)_2$. Evidence that the saccharide chains have a role in sequence specificity. *J. Mol. Biol. 231*, 753–767.
15. Hou, M. H., Robinson, H., Gao, Y. G., and Wang, A. H.-J. (2004) Crystal structure of the [Mg^{2+}−$(chromomycin\ A_3)_2$]−$d(TTGGCCAA)_2$ complex reveals GGCC binding specificity of the drug dimer chelated by a metal ion. *Nucleic Acids Res. 32*, 2214–2222.
16. Hou, M. H., and Wang, A. H.-J. (2005) Mithramycin forms a stable dimeric complex by chelating with Fe(II): DNA-interacting characteristics, cellular permeation and cytotoxicity. *Nucleic Acids Res. 33*, 1352–1361.
17. Chakrabarti, S., Bhattacharyya, D., and Dasgupta, D. (2000) Structural basis of DNA recognition by anticancer antibiotics, chromomycin A_3, and mithramycin: Roles of minor groove width and ligand flexibility. *Biopolymers 56*, 85–95.
18. Devi, P. G., Pal, S., Banerjee, R., and Dasgupta, D. (2007) Association of antitumor antibiotics, mithramycin and chromomycin, with Zn(II). *J. Inorg. Biochem. 101*, 127–137.
19. Itzhaki, L., Weinberger, S., Livnah, N., and Berman, E. (1990) A unique binding cavity for divalent cations in the DNA−metal−chromomycin A_3 complex. *Biopolymers 29*, 481–489.
20. Majee, S., Sen, R., Guha, S., Bhattacharyya, D., and Dasgupta, D. (1997) Differential interactions of the Mg^{2+} complexes of chromomycin A_3 and mithramycin with poly(dG-dC) × poly(dC-dG) and poly(dG) × poly(dC). *Biochemistry 36*, 2291–2299.
21. Cantor, C. R., and Tinoco, I., Jr. (1965) Absorption and optical rotatory dispersion of seven trinucleoside diphosphates. *J. Mol. Biol. 13*, 65–77.
22. Hou, M. H., Robinson, H., Gao, Y. G., and Wang, A. H.-J. (2002) Crystal structure of actinomycin D bound to the CTG triplet repeat sequences linked to neurological diseases. *Nucleic Acids Res. 30*, 4910–4917.
23. Hou, M. H., Lin, S. B., Yuann, J. M., Lin, W. C., Wang, A. H.-J., and Kan, L. S. (2001) Effects of polyamines on the thermal stability and formation kinetics of DNA duplexes with abnormal structure. *Nucleic Acids Res. 29*, 5121–5128.
24. Shiraishi, H., Kataoka, M., Morita, Y., and Umemoto, J. (1993) Interactions of hydroxyl radicals with tris (hydroxymethyl) aminomethane and Good's buffers containing hydroxymethyl or hydroxyethyl residues produce formaldehyde. *Free Radical Res. Commun. 19*, 315–321.
25. Cons, B. M., and Fox, K. R. (1989) Interaction of mithramycin with metal ions and DNA. *Biochem. Biophys. Res. Commun. 160*, 517–524.
26. Huang, H. W., Li, D., and Cowan, J. A. (1995) Biostructural chemistry of magnesium. Regulation of mithramycin−DNA interactions by Mg^{2+} coordination. *Biochimie 77*, 729–738.
27. Mucha, A., Cappanelli, M., Szczepanik, W., Kaczmarek, P., Skala, J., and Jezowska-Bojczuk, M. (2006) Influence of the physiologically widespread substances on the oxidative activity of copper(II) complexes with sinefungin, a nucleoside antibiotic. *J. Inorg. Biochem. 100*, 178–185.
28. Espey, D. K., Wu, X. C., Swan, J., Wiggins, C., Jim, M. A., Ward, E., Wingo, P. A., Howe, H. L., Ries, L. A., Miller, B. A., Jemal, A., Ahmed, F., Cobb, N., Kaur, J. S., and Edwards, B. K. (2007) Annual report to the nation on the status of cancer, 1975–2004, featuring cancer in American Indians and Alaska Natives. *Cancer 110*, 2119–2152.
29. Shannon, R. D. (1976) Revised effective ionic radii and systematic studies of interatomic distances in halides and chalcogenides. *Acta Crystallogr., Sect. A: Found. Crystallogr. 32*, 751–767.
30. Gaboriau, F., Kreder, A., Clavreul, N., Moulinoux, J. P., Delcros, J. G., and Lescoat, G. (2004) Polyamine modulation of iron uptake in CHO cells. *Biochem. Pharmacol. 67*, 1629–1637.
31. Liu, C., and Chen, F. M. (1994) Oligonucleotide studies of sequence-specific binding of chromomycin A_3 to DNA. *Biochemistry 33*, 1419–1424.
32. Berman, H. M. (1997) Crystal studies of B-DNA: The answers and the questions. *Biopolymers 44*, 23–44.
33. Moravek, Z., Neidle, S., and Schneider, B. (2002) Protein and drug interactions in the minor groove of DNA. *Nucleic Acids Res. 30*, 1182–1191.

34. Darnell, J. E., Jr. (2002) Transcription factors as targets for cancer therapy. *Nat. Rev. Cancer 2*, 740–749.
35. Wu, J., Ling, X., Pan, D., Apontes, P., Song, L., Liang, P., Altieri, D. C., Beerman, T., and Li, F. (2005) Molecular mechanism of inhibition of survivin transcription by the GC-rich sequence-selective DNA binding antitumor agent, hedamycin: Evidence of survivin down-regulation associated with drug sensitivity. *J. Biol. Chem. 280*, 9745–9751.
36. Snyder, R. C., Ray, R., Blume, S., and Miller, D. M. (1991) Mithramycin blocks transcriptional initiation of the c-myc P1 and P2 promoters. *Biochemistry 30*, 4290–4297.
37. Remsing, L. L., Bahadori, H. R., Carbone, G. M., McGuffie, E. M., Catapano, C. V., and Rohr, J. (2003) Inhibition of c-src transcription by mithramycin: Structure−activity relationships of biosynthetically produced mithramycin analogues using the c-src promoter as target. *Biochemistry 42*, 8313–8324.
38. Lindqvist, M., and Graslund, A. (2001) An FTIR and CD study of the structural effects of G-tract length and sequence context on DNA conformation in solution. *J. Mol. Biol. 314*, 423–432.
39. Goodsell, D. S., Kopka, M. L., Cascio, D., and Dickerson, R. E. (1993) Crystal structure of CATGGCCATG and its implications for A-tract bending models. *Proc. Natl. Acad. Sci. U.S.A. 90*, 2930–2934.
40. Yang, X. L., and Wang, A. H.-J. (1999) Structural studies of atom-specific anticancer drugs acting on DNA. *Pharmacol. Ther. 83*, 181–215.
41. Tadolini, B., and Cabrini, L. (1990) The influence of pH on OH. Scavenger inhibition of damage to deoxyribose by Fenton reaction. *Mol. Cell. Biochem. 94*, 97–104.
42. Bruice, T. C., Zipplies, M. F., and Lee, W. A. (1986) The pH dependence of the mechanism of reaction of hydrogen peroxide with a nonaggregating, non-μ-oxo dimer-forming iron (III) porphyrin in water. *Proc. Natl. Acad. Sci. U.S.A. 83*, 4646–4649.
43. Capranico, G., Zagotto, G., and Palumbo, M. (2004) Development of DNA topoisomerase-related therapeutics: A short perspective of new challenges. *Curr. Med. Chem. Anticancer Agents 4*, 335–345.
44. Zwelling, L. A. (1989) Topoisomerase II as a target of antileukemia drugs: A review of controversial areas. *Hematol. Pathol. 3*, 101–112.
45. Staker, B. L., Feese, M. D., Cushman, M., Pommier, Y., Zembower, D., Stewart, L., and Burgin, A. B. (2005) Structures of three classes of anticancer agents bound to the human topoisomerase I-DNA covalent complex. *J. Med. Chem. 48*, 2336–2345.
46. Rothenberg, M. L. (1997) Topoisomerase I inhibitors: Review and update. *Ann. Oncol. 8*, 837–855.
47. Pommier, Y. (2006) Topoisomerase I inhibitors: Camptothecins and beyond. *Nat. Rev. Cancer 6*, 789–802.
48. Bugreev, D. V., Vasyutina, E. L., Ryabinin, V. A., Sinyakov, A. N., Buneva, V. N., and Nevinsky, G. A. (2001) Inhibition of human DNA topoisomerase I by new DNA minor groove ligands: Derivatives of oligo-1,3-thiazolecarboxamides. *Antisense Nucleic Acid Drug Dev. 11*, 137–147.
49. Sanmartin, C., Font, M., and Palop, J. A. (2006) Molecular symmetry: A structural property frequently present in new cytotoxic and proapoptotic drugs. *Mini-Reviews Med. Chem. 6*, 639–650.

BI701915F